

Accelerating Wireless Federated Learning via Nesterov's Momentum and Distributed Principle Component Analysis

Yanjie Dong, *Member, IEEE*, Luya Wang, Yuanfang Chi, *Student Member, IEEE*,
Jia Wang, *Member, IEEE*, Haijun Zhang, *Fellow, IEEE*, Fei Richard Yu, *Fellow, IEEE*,
Victor C. M. Leung, *Life Fellow, IEEE*, Xiping Hu, *Member, IEEE*

Abstract

A wireless federated learning system is investigated by allowing a server and workers to exchange uncoded information via orthogonal wireless channels. Since the workers frequently upload local gradients to the server via bandwidth-limited channels, the uplink transmission from the workers to the server becomes a communication bottleneck. Therefore, a one-shot distributed principle component analysis (PCA) is leveraged to reduce the dimension of uploaded gradients such that the communication bottleneck is relieved. A PCA-based wireless federated learning (PCA-WFL) algorithm and its accelerated version (i.e., PCA-AWFL) are proposed based on the low-dimensional gradients and the Nesterov's momentum. For the non-convex loss functions, a finite-time analysis is performed to quantify the impacts of system hyper-parameters on the convergence of the PCA-WFL and PCA-AWFL algorithms. The PCA-AWFL algorithm is theoretically certified to converge faster than the PCA-WFL algorithm. Besides, the convergence rates of PCA-WFL and PCA-AWFL algorithms quantitatively reveal the linear speedup with respect to the number of workers over the vanilla gradient descent algorithm. Numerical results are used to demonstrate the improved convergence rates of the proposed PCA-WFL and PCA-AWFL algorithms over the benchmarks.

Y. Dong and X. Hu are with the Faculty of Engineering, Shenzhen MSU-BIT University, Shenzhen, China.

L. Wang and J. Wang are with the College of Computer Science and Software Engineering, Shenzhen University, Shenzhen, China.

H. Zhang is with Beijing Advanced Innovation Center for Materials Genome Engineering, Beijing Engineering and Technology Research Center for Convergence Networks and Ubiquitous Services, Institute of Artificial Intelligence, University of Science and Technology Beijing, Beijing, China.

F. R. Yu is with the College of Computer Science and Software Engineering, Shenzhen University, Shenzhen, China and the Department of Systems and Computer Engineering, Carleton University, Ottawa, Canada.

Y. Chi and V. C. M. Leung is with the College of Computer Science and Software Engineering, Shenzhen University, Shenzhen, China, and the Department of Electrical and Computer Engineering, The University of British Columbia, Vancouver, Canada.

Index Terms

Federated learning, distributed principle component analysis, momentum acceleration.

NOMENCLATURE

Scalars Definitions

$h_{n,k}$	Channel coefficient vector of worker n per frame k
h_0	Channel truncation threshold
d_0 and \hat{d}_0	Dimension and reduced dimension of data sample
d_1	Dimension of model parameter
$c_{n,k}$	Inverse of channel scheduling probability of worker n per frame k
η	Learning rate
L	Lipschitz constant
β	Momentum factor
K	Number of frames
M	Number of samples per worker
N	Number of workers
α	Pathloss exponent
$\rho_{n,k}$	Power control factor of worker n per frame k
σ^2	Power of additive white Gaussian noise (AWGN)
c_1 and c_2	Predetermined constants
$\delta_{n,k}$	Propagation distance of worker n per frame k
p_0	Transmit power budget of each worker
G	Upper bound of gradient variance

Vectors

z_k	Accumulated noise per frame k
u_k and v_k	Auxiliary variables per frame k
$\mathbb{1}_{n,k}$	Scheduling policy of worker n per frame k
w_k	Global model per frame k
$y_{n,k}$	Gradient of worker n per frame k
$p_{n,k}$	Power control vector of worker n per frame k
$z_{n,k}$	Real part of AWGN
$\hat{a}_{m,n}$	The m th low-dimensional sample of worker n

$\nabla_{n,k}$ The n th intermittent gradient per frame k

$\hat{\nabla}_{n,k}$ The n th received gradient per frame k

Matrices

\hat{U} First \hat{d}_0 columns of global left-singular matrix

U and V Global left- and right-singular matrices

Λ and Λ_n Global and local principle component matrices

U_n and V_n Local left- and right-singular matrices of worker n

A_n and \hat{A}_n Local and low-dimensional datasets of worker n

Functions

$f(\cdot)$ Empirical risk

$f_n(\cdot)$ Local loss function of worker n

I. INTRODUCTION

With the sheer volume of data at wireless edge terminals, the world starts to embrace machine intelligence applications at network edges (a.k.a., edge intelligence) [1]. As a popular framework of edge intelligence, a wireless federated learning (WFL) system can jointly infer knowledge from the proliferating data at edge terminals via the orchestration of cloud servers [2]. By decoupling the learning process from the data collecting process, the WFL system can reduce the exposure of private information and provide immediate access to global models for the wireless terminals [3]. Several emerging topics were investigated in the WFL system to improve the communication efficiency [4], [5], to enhance the robustness over passive and proactive adversaries [6], [7], and to reduce the content access delay [8], [9]. For example, the lazy aggregation [4] and quantized lazy aggregation [5] are proposed to adaptively reduce the required communication rounds for training models in the WFL system. **Since training deep neural networks becomes available for edge terminals, a federated learning-to-optimize framework was conceptualized for solving the NP-hard radio resource allocation problem by exploiting local data at all edge terminals [10].**

While the aforementioned works are based on an error-free WFL system, the impacts of noise and fadings of wireless channels remain under-exploited on the energy consumption, communication efficiency, and convergence rate of the WFL system [11]. In this work, we aim at: 1) designing supervised learning algorithms for the WFL system (or WFL algorithms for brevity) to adapt to the wireless channels; and, 2) quantifying the impacts of the noise and fadings on the convergence rates of our proposed WFL algorithms.

Related works and motivations. When the federated learning system is deeply coupled with wireless communications, the success of WFL algorithms requires to adapting to the wireless channels and to suitably

using the scarce radio resources [11]. There are two concurrent research directions for the WFL system, i.e., the digital WFL system [12], [13] and the analog WFL system [14], [15]. Since the digital WFL system uses the digital modulations to provide reliable communication tunnels, the joint design of WFL algorithms and radio resource management algorithms is required to efficiently utilize the radio resources for training. More specifically, in the digital WFL system, radio resource allocation algorithms were designed to optimize the training loss [16], [17], training efficiency [18], [19], training duration [20]–[22], consumed energy [23], the number of correctly received model parameters per unit duration [24] as well as the tradeoff between training duration and consumed energy [25]. For example, the worker selection and bandwidth were jointly allocated to minimize the training loss in a hierarchical digital WFL system in [17]. A joint resource allocation of the minibatch size, uplink and downlink duration of workers was proposed to maximize the learning efficiency of the digital WFL system [19]. By opportunistically scheduling workers, the number of selected workers and the training duration could be respectively optimized in [13] and [21] for the digital WFL system. Besides, the interplay between the reconfigurable intelligent surfaces (RISs) and the federated learning was investigated to enhance the spectrum-sensing accuracy and reliability of the training process by jointly allocating RIS association, wireless bandwidth, and phase-shifts of RISs [24]. The covert digital WFL system was investigated by jamming the potential eavesdroppers while striking a balance between training accuracy and energy consumption [25]. The gradient quantization codebook was designed in [26] for the digital WFL system. Note that the design of radio resource management algorithms for computation-limited workers (e.g., tiny machine learning workers and sensors) could be a challenging task.

Without requiring complex radio resource management, the over-the-air computing (OAC) technology allows the analog WFL system to aggregate the analog modulated local gradients by exploiting the waveform superposition property. In this vein, the analog WFL algorithms were proposed to adapt the information exchange to the AWGN channels [14], [27] and fading channels [28]–[34]. The signal encoding algorithms were designed for the analog WFL system [30], [35], [36]. For example, the channel noise is exploited to preserve the privacy of workers in the analog WFL system [28]. The uncoded and coded transmission were respectively exploited in [29] and [30] to develop analog WFL algorithms, where the received strength of local gradients is limited by the farthest worker. The proposed analog WFL algorithm in [14] averages the local gradients by assuming the same variance of local gradients, and recovers the average gradient via an approximate message passing mechanism. Besides, the momentum term is used to accelerate the analog WFL algorithm for (strongly) convex loss functions [32]. In order to achieve the drastic reduction of required bandwidth via the OAC technology, the aforementioned analog WFL algorithms need to obtain the unbiased estimators of the global model and global gradient by strong assumptions: 1) the independent

and identically-distributed (i.i.d.) local gradients [14]; or 2) i.i.d. locations of workers [27]–[33]. Besides, the finite-time analysis was only performed for (strongly) convex loss functions [14], [27], [28], [32], [33]. Motivated by these facts, we envision that the potential application scenarios of the analog WFL system can be increased by removing the i.i.d. assumptions on local gradients and workers while calculating the global model and the global gradient.

Contributions. Different from [14], [27]–[33], we consider the non-i.i.d. local gradients and the non-i.i.d. locations of workers. We aim at developing and analyzing the analog WFL algorithms for the non-convex loss functions. For the ease of implementation, we allow the workers to upload local gradients to the server via uncoded pulse amplitude modulation. When the workers have non-i.i.d. locations, the propagation distances between the workers and server are in high variance. Since the OAC technology has a limited degree of freedom for power control, the received strength of local gradients is confined by the farthest worker. Otherwise, the workers that are close to the server can scale their local gradients with larger factors than workers farther away (i.e., the near-far effect of co-channel transmission) [37]. To remove the limitations of non-i.i.d. location of workers, the orthogonal channel usages¹ are allowed at workers. Due to the scarcity of radio resources, we leverage a one-shot distributed principle component analysis (PCA) algorithm [38] to reduce the dimension of samples and thereby the dimension of local gradients. The detailed contributions of our work are summarized as follows.

- We aim at developing analog WFL algorithms that can handle the near-far effect of workers and inherit the simplicity of uncoded pulse amplitude modulation. We leverage a one-shot distributed PCA algorithm [38] to reduce the dimension of samples and thereby the required radio resource.
- We introduce a truncated channel inversion to construct an unbiased estimator of the global gradient when the workers have non-i.i.d. locations. Based on the introduced truncated channel inversion and the one-shot distributed PCA, we start by proposing PCA-WFL algorithm for the non-convex loss functions. Motivated by the potential speedup capability of Nesterov’s momentum, we propose a PCA-based accelerated WFL (PCA-AWFL) algorithm. Leveraging the intelligence networking [1], we also give an intuition on the potential speedup capability of Nesterov’s momentum.
- Our theoretical results reveal that the PCA-AWFL algorithm converges with a faster rate than the PCA-WFL algorithm at an expense of a larger error-floor term. Besides, our theoretical results also confirm that the PCA-WFL and PCA-AWFL algorithms can benefit from the computational parallelism of numerous workers.

¹Since each frame consists of multiple resource elements that are temporally and spectrally orthogonal, a *channel usage* indicates a utilization of each temporally-and-spectrally orthogonal resource element in the frame.

Several numerical tests are performed to verify the performance of our proposed PCA-WFL and PCA-AWFL algorithms on the FMNIST dataset [39], CIFAR-10 dataset [40], and AWE dataset [41].

Organization and notations. The remaining work is organized as follows. Several preliminaries are introduced in Section II. The system model and problem description are provided in Section III. The algorithm design and corresponding finite-time analysis are established in Section IV. Numerical results are presented to verify the theoretical results in Section V, which is followed by the concluding remarks in Section VI.

Notations. The vectors and matrices are respectively denoted by lowercase letters and uppercase letters. The operator \odot denotes the Hadamard product, and the operator $\mathbb{E}[\cdot]$ denotes the expectation. The operators $|\cdot|$ and $\|\cdot\|$ respectively denote the absolute value and the ℓ_2 -norm. The terms \mathbb{C} and \mathbb{R} are the set of complex values and the set of real values, respectively.

II. PRELIMINARIES

A. One-shot Distributed PCA

As one of the dimension reduction algorithms, PCA is widely used due to its simplicity in implementation and the preservation of the most characteristics of the original dataset [42]. Note that the PCA requires to perform singular-value decomposition (SVD) to the original dataset $A \in \mathbb{R}^{d_0 \times M}$ with d_0 and M as the dimension and number of samples, respectively. However, the SVD operation cannot be implemented in WFL systems. The reasons are as follows: 1) the original dataset A is split across multiple workers; and 2) the server is not allowed to collect data samples from workers in the WFL systems. Although an iterative distributed PCA is proposed in [15], a one-shot distributed PCA [38] is preferred in the WFL systems to save the scarce radio resource.

To facilitate the investigation of a WFL system with high-dimensional datasets, we start with reviewing the one-shot distributed PCA. We refer readers to sources [38], [43] for more details. Suppose that each worker n has M samples as $A_n \in \mathbb{R}^{d_0 \times M}$. The original dataset A is thus denoted by $A = [A_1, A_2, \dots, A_N] \in \mathbb{R}^{d_0 \times MN}$. We summarize the one-shot distributed PCA in Algorithm 1.

When \hat{d}_0 is carefully selected, each low-dimensional local dataset $\hat{A}_n \in \mathbb{R}^{\hat{d}_0 \times M}$ can preserve the most important information for training [38, Theorem 9].

We perform a budget calculation to illustrate the benefits of the one-shot distributed PCA as in Fig. 1. We consider to train a three-layer perceptron to classify the FMNIST dataset [39]. Suppose that the input, hidden, and output layers respectively have d , 64, and 10 neurons with d denoting the dimension of the data sample. The numbers of model parameters between the input layer and the hidden layer are,

Algorithm 1 One-shot Distributed PCA Algorithm

- 1: Each worker n performs the SVD to local dataset $A_n = U_n \Lambda_n V_n^T$
 - 2: Each worker n uploads the first \hat{d}_0 columns of $U_n \Lambda_n$ to the server
 - 3: The server performs the SVD to the collected matrix $[U_1 \Lambda_1, U_2 \Lambda_2, \dots, U_N \Lambda_N] = U \Lambda V^T$
 - 4: The server obtains the first \hat{d}_0 columns of U as $\hat{U} = U[1 : \hat{d}_0]$
 - 5: The server broadcasts the matrix \hat{U} to N workers
 - 6: Each worker n performs the dimension reduction of local dataset as $\hat{A}_n = \hat{U}^T A_n$
-

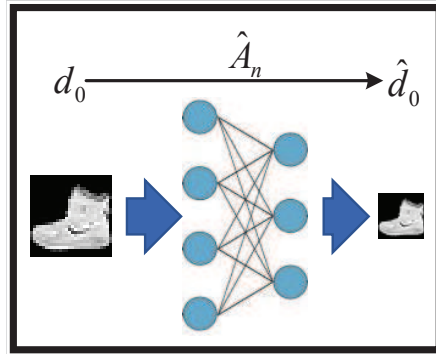


Fig. 1: Mapping a d_0 -dimensional figure to a \hat{d}_0 -dimensional figure based on the one-shot distributed PCA.

respectively, $64(d_0 + 1)$ and $64(\hat{d}_0 + 1)$ before and after the one-shot distributed PCA. When both \hat{d}_0 and d_0 are sufficiently large with $\hat{d}_0 \leq d_0$, the dimension of exchanged information is reduced by approximately $1 - \hat{d}_0/d_0$ per frame. Note that d_0 is 784 for the FMNIST dataset. When we set $\hat{d}_0 = 500$, the communication saving is 36.22% per frame. We will illustrate the impacts of the dimension reduction on the learning performance in the numerical results.

The one-shot distributed PCA algorithm can reduce the demand for wireless channels of our proposed algorithms, and thereby increase the potential application scenarios.

B. Intelligence Quantification

Different generations of networking technologies establish cooperation of human beings by allowing the movement of “something”, such as matter, energy, and information [1]. The next generation of networking technology is built upon a higher level abstraction of the current one. For example, the energy quantifies a matter’s moving speed, and information quantifies the energy dispersal speed. Therefore, we can envision that a new networking technology can provide a higher abstraction of information, namely, intelligence. Mimicking the ways to define energy in Thermodynamics and information in Shannon’s entropy, it is

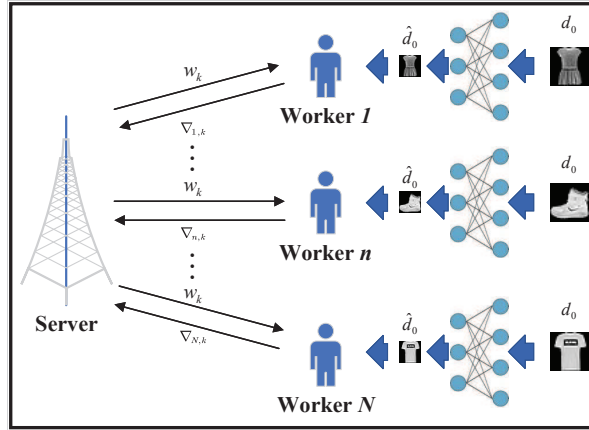


Fig. 2: An illustration of WFL system with one-shot distributed PCA.

suggested that the difference of intelligence can be defined as $dw = dS/dR$ where S denotes the similarity of the current and the optimal orders, and R is the concerned parameter [1]. When the concerned parameter R is time in a supervised learning task, the difference of intelligence is specified as $dw/dt = -\nabla f(w)$ with the gradient of empirical risk function $\nabla f(w)$ [44]. Therefore, we are motivated to perform the finite-time analysis of the time-average variance of intelligence's difference to quantify the spread speed of intelligence in the investigated WFL system.

III. SYSTEM MODEL AND PROBLEM DESCRIPTION

In this section, we present an analog WFL system where multiple workers collaboratively learn a common model under the orchestration of a server. Since the difference of intelligence is contained in the gradient as discussed in Section II-B, we consider that the N workers upload the local gradients to the server for the model update over orthogonal wireless channels. After the global model update, the N workers download the global model from the server as shown in Fig. 2.

A. Problem Description

We consider a supervised learning task in the analog WFL system, where the server and N workers coordinately minimize the empirical risk as

$$\min_w f(w) := \frac{1}{N} \sum_{n=1}^N f_n(w) \quad (1)$$

where $f_n(w) = \frac{1}{M} \sum_{m=(n-1)M+1}^{nM} \ell(w; \hat{a}_{m,n})$ is the local loss of worker n with respect to the model $w \in \mathbb{R}^{d_1}$ and the sample $\hat{a}_{m,n} \in \mathbb{R}^{\hat{d}_0}$. More specifically, each $\hat{a}_{m,n}$ is the m th column of dataset \hat{A}_n .

B. Signal Model for Aggregated Gradient

In this work, we consider the non-line of sight Rayleigh fading uplink channels and the reliable downlink channel. Thus, each element of channel coefficient vector $h_{n,k} := [h_{n,k}[i]]_{i=1}^{d_1} \in \mathbb{C}^{d_1}$ follows an i.i.d. circularly symmetric complex Gaussian distribution $\mathcal{CN}(0, \delta_{n,k}^{-\alpha} I)$ with the propagation distance $\delta_{n,k}$ and the pathloss exponent α . Here, the value of d_1 denotes the number of channel usages and is equal to the dimension of the local gradient.

During the downlink period of frame k , the server broadcasts the model $w_k \in \mathbb{R}^{d_1}$ to all workers. In the uplink period per frame k , we allow each worker n to upload the n th local normalized gradient $y_{n,k}/\|y_{n,k}\|$ with $y_{n,k} := \nabla f_n(w_k) \in \mathbb{R}^{d_1}$ to the server as

$$\nabla_{n,k} = h_{n,k} \odot p_{n,k} \odot \frac{y_{n,k}}{\|y_{n,k}\|} + z_{n,k}, \forall n \quad (2)$$

where $p_{n,k} := [p_{n,k}[i]]_{i=1}^{d_1} \in \mathbb{C}^{d_1}$ is the power control vector of worker n per frame k with the i th element as $p_{n,k}[i]$, the operator \odot is the Hadamard product of two matrices, and $z_{n,k}$ is the real part of AWGN with mean zero and covariance matrix $\sigma^2 I$.

Following the uplink transmission in (2), the elements of the n th local normalized gradient are transmitted over orthogonal channel usages per frame k . Given the n th local gradient $y_{n,k}$, the transmit power of worker n over all channels is limited by

$$\left\| p_{n,k} \odot \frac{y_{n,k}}{\|y_{n,k}\|} \right\|^2 = p_0, \forall n \quad (3)$$

where p_0 is the power budget of each radio front-end.

When the i th channel usage of worker n experiences deep fading (i.e., $|h_{n,k}[i]| < h_0$) with h_0 as the predetermined truncation threshold, the i th channel usage cannot be used for information transmission by worker n . We define the scheduling policy by setting each element in $\mathbb{1}_{n,k} \in \mathbb{R}^{d_1}$ to one when the corresponding channel usage can be used by worker n per frame k (i.e., $|h_{n,k}[i]| \geq h_0$), and to zero otherwise. The expectation of each element $\mathbb{1}_{n,k}[i]$ is obtained as $\mathbb{E}[\mathbb{1}_{n,k}[i]] = \Pr[|h_{n,k}[i]| \geq h_0] = \exp(-\delta_{n,k}^\alpha h_0^2)$, which depends on the propagation distance of worker n and the truncation threshold h_0 . Since different channel usages experience an i.i.d. fadings, the worker n needs to avoid scaling different elements of the n th local normalized gradient by different channel power gains. Therefore, the workers perform power control such that each element in the n th received local normalized gradient is expected to be aligned with the same positive power control factor $\rho_{n,k}$. Different from [28]–[30], we perform channel alignment by considering the channel scheduling probability as

$$p_{n,k}[i] = \begin{cases} \rho_{n,k} c_{n,k} \frac{h_{n,k}^*[i]}{|h_{n,k}[i]|^2}, & |h_{n,k}[i]| \geq h_0 \\ 0, & |h_{n,k}[i]| < h_0 \end{cases} \quad (4)$$

where $c_{n,k}$ is the inverse of channel scheduling probability with $c_{n,k} := 1/\mathbb{E}[\mathbb{1}_{n,k}[i]] = \exp(\delta_{n,k}^\alpha h_0^2)$.

Substituting channel alignment policy (4) into (2), the n th intermittent gradient is obtained as

$$\nabla_{n,k} = \rho_{n,k} c_{n,k} \mathbb{1}_{n,k} \odot \frac{y_{n,k}}{\|y_{n,k}\|} + z_{n,k}, \forall n. \quad (5)$$

Based on (5), we have $\mathbb{E}[\nabla_{n,k}] = \rho_{n,k} y_{n,k}/\|y_{n,k}\|$ by recalling the facts $\mathbb{E}[\mathbb{1}_{n,k}[i]] = \exp(-\delta_{n,k}^\alpha h_0^2)$ and $c_{n,k} = 1/\mathbb{E}[\mathbb{1}_{n,k}[i]] = \exp(\delta_{n,k}^\alpha h_0^2)$. Note that the OAC technology only allows one single power control factor in the system, i.e., $\rho_k \equiv \rho_{n,k}$. Confined by the near-far effect of co-channel transmission, the received strength of local gradients is controlled by the farthest worker in the analog WFL systems [29], [30]. Therefore, the received strength for all workers can be extremely low when the propagation distance of the farthest worker is very large. In the investigated analog WFL system, each worker n uploads intermittent gradient $\nabla_{n,k}$ over orthogonal channel usages. Compared with the OAC technology, the investigated analog WFL system can use different power control factors $[\rho_{n,k}]_{n=1}^N$ to mitigate the the near-far effect of co-channel transmissions. We refer the removal of channel alignment factors as gradient alignment. After performing the gradient alignment by $\|y_{n,k}\|/\rho_{n,k}$, the n th received gradient is

$$\hat{\nabla}_{n,k} = c_{n,k} \mathbb{1}_{n,k} \odot y_{n,k} + \frac{z_{n,k}}{\rho_{n,k}} \|y_{n,k}\|, \forall n. \quad (6)$$

Denote the accumulated noise per frame k by $z_k = \frac{1}{N} \sum_{n=1}^N z_{n,k} \|y_{n,k}\|/\rho_{n,k}$ with $\mathbb{E}[z_k] = 0$. Based on (6), we obtain the aggregated gradient as

$$\frac{1}{N} \sum_{n=1}^N \hat{\nabla}_{n,k} = \frac{1}{N} \sum_{n=1}^N c_{n,k} \mathbb{1}_{n,k} \odot y_{n,k} + z_k. \quad (7)$$

Different from i.i.d. assumption on the propagation distance of workers [29]–[32], the received gradients in (7) show that our investigated analog WFL system factors in the propagation distances of workers.

IV. ALGORITHM DESIGN AND CONVERGENCE ANALYSIS

In this section, based on the following conditions on the local loss functions f_n , $n = 1, 2, \dots, N$, we develop the PCA-WFL algorithm and its accelerated version. Subsequently, we will analyze the convergence of our proposed algorithms.

Condition 1 (Bounded Variance of Gradient): Each local loss function is differentiable and has bounded gradient variance as $\frac{1}{N} \sum_{n=1}^N \|y_{n,k} - \nabla f(w_k)\|^2 \leq G$.

Condition 2 (Smoothness [45, eq. (1.2.11)]): Each local loss function has L -Lipschitz continuous gradient as

$$f_n(u) \leq f_n(w) + \langle \nabla f_n(w), u - w \rangle + \frac{L}{2} \|u - w\|^2 \quad (8)$$

where $u \in \mathbb{R}^{d_1}$ and $w \in \mathbb{R}^{d_1}$.

Condition 1 quantifies the deviation of local gradients from the global gradient [30]. Besides, Condition 1 is milder than the assumption on the bounded gradient in [14], [28]. Condition 2 requires the loss functions to be smooth and can be easily satisfied for some artificial neural networks [14], [28], [46].

Before starting the algorithm development, we introduce Lemma (1) to characterize the first-order and the second-order statistical properties of the aggregated gradient estimator (7).

Lemma 1: When Condition 1 is satisfied, the aggregated gradient (7) is an unbiased estimator of global gradient as

$$\mathbb{E}\left[\frac{1}{N}\sum_{n=1}^N\hat{\nabla}_{n,k}\right] = \frac{1}{N}\sum_{n=1}^N y_{n,k}. \quad (9)$$

The upper bound of the aggregated gradient per frame k is

$$\mathbb{E}\left[\left\|\frac{1}{N}\sum_{n=1}^N\hat{\nabla}_{n,k}\right\|^2\right] \leq 2\mathbb{E}[\|\nabla f(w_k)\|^2] + \frac{c_1 + c_2 d_1 \sigma^2 + 4G}{2N} \quad (10)$$

where $c_1 := \frac{1}{N}\sum_{n=1}^N[\exp(\delta_{n,k}^\alpha h_0^2) - 1]$ and $c_2 := \frac{1}{Np_0}\sum_{n=1}^N\delta_{n,k}^\alpha \exp(2\delta_{n,k}^\alpha h_0^2)E_1(\delta_{n,k}^\alpha h_0^2)$.

Proof: See Appendix A. □

Based on (9), Lemma 1 shows that the aggregated gradient (7) is an unbiased estimator of the global gradient when channel alignment policy (4) includes the channel scheduling policy. Based on (10), Lemma 1 also shows that the variance of the aggregated gradient is positively correlated to the propagation distances of workers $[\delta_{n,k}]_{n=1}^N$ and the truncation threshold h_0 .

A. PCA-WFL Algorithm

Using the aggregated gradient (7) and the one-shot distributed PCA, we present the PCA-WFL algorithm as

$$w_{k+1} = w_k - \eta \frac{1}{N} \sum_{n=1}^N \hat{\nabla}_{n,k} \quad (11)$$

where η is a stepsize.

We perform a finite-time analysis to obtain the convergence rate of the PCA-WFL algorithm in the following theorem, whose proof relies on Lemma 1.

Theorem 1: Assume that Conditions 1 and 2 are satisfied. When the stepsize η satisfies $\eta \leq 3/4L$, the convergence rate of the PCA-WFL algorithm is

$$\frac{1}{K} \sum_{k=0}^{K-1} \mathbb{E}[\|\nabla f(w_k)\|^2] = \mathcal{O}\left(\frac{1}{\eta K}\right) + \mathcal{O}\left(\frac{\eta}{N}\right) \quad (12)$$

where $\mathcal{O}(\frac{1}{\eta K})$ and $\mathcal{O}(\frac{\eta}{N})$ are respectively defined as

$$\mathcal{O}(\frac{1}{\eta K}) := \frac{4}{\eta K} \mathbb{E}[f(x_0) - f^*] \quad (13)$$

and

$$\mathcal{O}(\frac{\eta}{N}) := (c_1 + c_2 d_1 p_0^{-1} \sigma^2 + G) \frac{\eta L}{N}. \quad (14)$$

Proof: See Appendix C. □

Theorem 1 quantifies the variance of empirical risk's gradient over the total number of frames K , which reflects the spread of intelligence over different workers in finite-time horizon K for the PCA-WFL algorithm. The right-hand side (RHS) of (12) shows that the PCA-WFL algorithm converges at a rate $\mathcal{O}(1/\eta K)$ to an $\mathcal{O}(\eta/N)$ -neighbor (i.e., error-floor term) of the local optimal model for smooth non-convex empirical risk. Moreover, the size of the neighborhood is controlled by the stepsize η . Theorem 1 will serve as a benchmark to demonstrate the performance improvement of our proposed PCA-WFL algorithm.

B. Accelerating the PCA-WFL Algorithm

In this subsection, we leverage the prestigious Nesterov's momentum to accelerate the PCA-WFL algorithm. We start by giving an intuition on the acceleration capability of the Nesterov's moment based on Section II-B.

Recalling [47, eqs. (22)–(23)], the standard Nesterov's momentum recursion is

$$u_k = w_k - \eta \frac{1}{N} \sum_{n=1}^N \hat{\nabla}_{n,k} \quad (15a)$$

$$w_{k+1} = (1 + \beta)u_k - \beta u_{k-1} \quad (15b)$$

where u_k is a sequence of auxiliary variables.

However, the standard Nesterov's recursion in (15) cannot intuitively illustrate the speedup capability of the momentum term. Therefore, we provide an equivalent recursion of (15) as follows. Substituting (15a) into (15b) and performing several algebraic manipulations, we obtain

$$\eta \beta \frac{1}{N} \sum_{n=1}^N \hat{\nabla}_{n,k} = w_k - w_{k+1} - \eta \frac{1}{N} \sum_{n=1}^N \hat{\nabla}_{n,k} - \beta \left[w_{k-1} - w_k - \eta \frac{1}{N} \sum_{n=1}^N \hat{\nabla}_{n,k-1} \right]. \quad (16)$$

Setting

$$\eta \beta u_{k+1} := w_k - w_{k+1} - \eta \frac{1}{N} \sum_{n=1}^N \hat{\nabla}_{n,k} \quad (17)$$

and

$$v_k := \beta u_{k+1} + \frac{1}{N} \sum_{n=1}^N \hat{\nabla}_{n,k}. \quad (18)$$

Based on (16)–(18), we obtain $w_{k+1} = w_k - \eta v_k$ and $u_{k+1} = \beta u_k + \frac{1}{N} \sum_{n=1}^N \hat{\nabla}_{n,k}$. Therefore, we recast the recursion (15) as

$$u_{k+1} = \beta u_k + \frac{1}{N} \sum_{n=1}^N \hat{\nabla}_{n,k} \quad (19a)$$

$$v_k = \beta u_{k+1} + \frac{1}{N} \sum_{n=1}^N \hat{\nabla}_{n,k} \quad (19b)$$

$$w_{k+1} = w_k - \eta v_k \quad (19c)$$

where β is a momentum factor.

Applying the recursion in (19a) with $u_0 = 0$, we obtain

$$u_k = \sum_{t=0}^{k-1} \beta^{k-1-t} \frac{1}{N} \sum_{n=1}^N \hat{\nabla}_{n,t}. \quad (20)$$

Substituting (19b) and (20) into (19c), we obtain

$$\begin{aligned} & \frac{1}{\eta} (w_k - w_{k+1}) \\ &= (1 + \beta) \frac{1}{N} \sum_{n=1}^N \hat{\nabla}_{n,k} + \sum_{t=0}^{k-1} \beta^{k+1-t} \frac{1}{N} \sum_{n=1}^N \hat{\nabla}_{n,t}. \end{aligned} \quad (21)$$

We observe that (21) updates model w_k via a momentum-based aggregated gradient and the discounted historical aggregated gradients while the PCA-WFL algorithm only uses the received gradient. Section II-B indicates that the spread of intelligence is contained in the gradient of empirical risk, which is the aggregated gradient in the investigated analog WFL system. Therefore, the Nesterov's momentum can speed up the PCA-WFL algorithm by exploiting more intelligence from the historical aggregated gradients.

Combining (19) with the one-shot distributed PCA, we summarize the procedures of our proposed PCA-AWFL algorithm in Algorithm 2. Different from [14], exchanging the normalized gradients reduces the steps for mean value removal for the received gradients.

Remark 1 (Link Budget Analysis): Each worker n needs to upload the local normalized gradient $y_{n,k}/\|y_{n,k}\|$ and the gradient alignment factor $\|y_{n,k}\|/\rho_{n,k}$ to the server. Therefore, the channel usage per worker n is $d_1 + 1$, and the total channel usage for each global gradient aggregation is $N(d_1 + 1)$.

Leveraging Lemma 1, we establish the convergence rate of our proposed PCA-AWFL algorithm.

Theorem 2: Assume that the Conditions 1 and 2 are satisfied, and $u_0 = 0$. When the stepsize η and momentum factor β satisfy $\eta \leq 3(1-\beta)^2/2(2+\beta^3)L$, the PCA-AWFL algorithm converges at a rate of

$$\frac{1}{K} \sum_{k=0}^{K-1} \mathbb{E}[\|\nabla f(w_k)\|^2] = \mathcal{O}\left(\frac{1-\beta}{\eta K}\right) + \mathcal{O}\left(\frac{\eta}{N(1-\beta)^2}\right) \quad (23)$$

Algorithm 2 PCA-AWFL Algorithm

- 1: **Initialization:** Momentum factor β , stepsize η , and initial values $u_0 = 0$
 - 2: The server and workers cooperatively perform the Algorithm 1 to reduce the dimension of local datasets
 - 3: **for** $k = 1, \dots, \infty$ **do**
 - 4: The server broadcasts the model vector w_k to all workers
 - 5: Each worker n estimates the channel coefficient vector $h_{n,k}$ and the inverse of channel scheduling probability $c_{n,k}$
 - 6: Each worker n sets the channel alignment factor as

$$\frac{1}{\rho_{n,k}^2} = \frac{c_{n,k}^2}{p_0} \sum_{i=1}^{d_1} \frac{|\mathbb{1}_{n,k}[i]y_{n,k}[i]|^2}{|h_{n,k}[i]|^2 \|y_{n,k}\|^2} \quad (22)$$
 - 7: Each worker n performs the channel alignment in (4)
 - 8: Each worker n uploads to the server the local normalized gradient $y_{n,k}/\|y_{n,k}\|$
 - 9: The server performs gradient alignment by using $[\|y_{n,k}\|/\rho_{n,k}]_{n=1}^N$ and updates model via (19)
 - 10: **end for**
-

where $\mathcal{O}(\frac{1-\beta}{\eta K})$ and $\mathcal{O}(\frac{\eta}{N(1-\beta)^2})$ are respectively defined as

$$\mathcal{O}(\frac{1-\beta}{\eta K}) := \frac{4(1-\beta)}{\eta K} \mathbb{E}[f(x_0) - f^*] \quad (24)$$

and

$$\mathcal{O}(\frac{\eta}{N(1-\beta)^2}) := (c_1 + c_2 d_1 p_0^{-1} \sigma^2 + G) \frac{\eta L}{N(1-\beta)^2}. \quad (25)$$

Proof: See Appendix D. □

Based on (23), we observe that our proposed PCA-AWFL algorithm converges to an $\mathcal{O}(\eta/N(1-\beta)^2)$ -neighbor (i.e., the error-floor term) of local optima at a rate $\mathcal{O}((1-\beta)/\eta K)$ for smooth non-convex empirical risk. Based on (25), we have three observations: 1) the error-floor term decreases with the number of workers N ; 2) the error-floor term shrinks with stepsize η at the expense of slow convergence; and 3) the error-floor term increases with the distances of workers to the server. Compared with Theorem 1, we observe from Theorem 2 that our proposed PCA-AWFL algorithm converges faster than the PCA-WFL algorithm by a factor of $1 - \beta$ at the expense of an error-floor term $\mathcal{O}(\eta/N(1-\beta)^2)$ -neighbor. When the momentum term β reduces to zero, the PCA-AWFL reduces to PCA-WFL.

When the value K is sufficiently large, we can set $\eta = \sqrt{N/K}$ such that $\eta \leq 3(1-\beta)^2/2(2+\beta^3)L$. Based on the RHS of (23), we can set $\eta = \sqrt{N/K}$ such that

$$\frac{1}{K} \sum_{k=0}^{K-1} \mathbb{E}[\|\nabla f(w_k)\|^2] = \mathcal{O}\left(\frac{1}{\sqrt{NK}}\right). \quad (26)$$

Eq. (26) shows that our proposed PCA-AWFL achieves a linear speedup with respect to the number of workers.

Theorems 1 and 2 show that the gradient norms of the PCA-WFL and PCA-AWFL algorithms become stable such that no more intelligence can be dispersed among the workers. We envision that the testing accuracies of PCA-WFL and PCA-AWFL algorithms reach the peaks when the intelligence stops spreading.

V. NUMERICAL RESULTS

We perform the numerical experiments to show the performance comparison between our proposed algorithms and the benchmarks. In the numerical experiments, we use the FMNIST dataset [39], CIFAR-10 dataset [40], and AWE dataset [41]. The FMNIST dataset contains 10-class grayscale images of fashion products with 60,000 training samples and 10,000 testing samples. The CIFAR-10 dataset contains 10-class tiny color images with 50,000 training samples and 10,000 testing samples. The AWE dataset is obtained by performing a destructive experiment for automatic washing equipment of high-speed railway vehicles with 21,047 training samples and 2,352 testing samples. The samples of the AWE dataset belong to six categories. The training samples are homogeneously distributed among the workers, and all the testing samples are placed on the server.

1) *Benchmark Descriptions:* Three benchmarks are considered: the PCA based error-free batch gradient descent (PCA-EF), PCA based error-free Adam (PCA-EF-Adam), and PCA Adam (PCA-Adam) algorithms. More specifically, the PCA-EF algorithm allows the workers to reduce the dimension of data via the one-shot distributed PCA and to upload all local gradients to the server via error-free channels. The PCA-EF-Adam algorithm differs from the PCA-EF by using an advanced Adam solver. The PCA-Adam algorithm requires the workers to upload all local gradients via the Rayleigh fading channels.

2) *Deployment Analysis:* For the FMNIST dataset, we consider to train a three-layer perceptron with a 64-neuron hidden layer and a 10-neuron output layer, respectively. For the CIFAR-10 dataset, we consider to train a neural network that consists of a 1D-convolutional layer, a 64-neuron hidden layer, and a 10-neuron output layer. The 1D-convolutional layer contains a 7×1 filter. For the CIFAR-10 dataset, we preprocess the data samples via a pretrained AlexNet [48] for the convenience of PCA operations. For the AWE dataset, we consider to train a three-layer perceptron with a 128-neuron hidden layer and a 6-neuron

output layer, respectively. The hyperbolic tangent activation function is used at the hidden layer, and the loss function is the softmax cross entropy. The computational complexities for neural networks can be obtained based on [49, Appendix A.1]. In this work, we estimate the computational complexity of neural networks for three different datasets and different input sizes via the python package *thop*. The results are shown in Table I. We observe that the neural network for AWE with 1,024-dimensional input has the highest computational complexity—131,840 FLOPs. Multiplying by the number of frames, we obtain the worst-case overall complexity is around 3.96×10^9 FLOPs. Note that a Raspberry Pi-4B (4GB) 64-bit has a 2.02×10^9 FLOPs per second per watt². The 3.96×10^9 FLOPs requirement can be well handled by current off-the-shelf energy-limited terminals that have 2.02×10^9 FLOPs per second per watt. Therefore, we believe that our proposed PCA-WFL and PCA-AWFL algorithms are suitable to be deployed at the off-the-shelf edge terminals in real-life applications.

TABLE I: Computational Complexity of Neural Networks.

AWE		CIFAR-10		FMNIST	
\hat{d}_0	FLOPs	\hat{d}_0	FLOPs	\hat{d}_0	FLOPs
100	13,568	100	7,484	300	19,584
300	39,168	200	14,584	400	25,984
500	64,768	300	21,684	500	32,384
700	90,368	400	28,784	600	38,784
900	115,968	500	35,884	700	45,184
1024	131,840	600	42,984	784	50,560

3) *Parameter Setup*: For the FMNIST dataset, the analog WFL system has six workers with the propagation distances as 416.33 meters, 435.07 meters, 389.01 meters, 475.76 meters, 251.43 meters, and 163.21 meters. For the CIFAR-10 and AWE datasets, the analog WFL system has twelve workers with the propagation distances as 284.43 meters, 396.79 meters, 407.76 meters, 444.18 meters, 465.94 meters, 438.90 meters, 206.80 meters, 435.08 meters, 280.54 meters, 183.13 meters, 460.88 meters, and 362.27 meters. The values of \hat{d}_0 are respectively set as 500 for the FMNIST dataset, 400 for the CIFAR-10 dataset, and 700 for the AWE dataset. The momentum factors β are respectively set as 0.95 for the FMNIST dataset, 0.85 for the CIFAR-10 dataset, and 0.9 for the AWE dataset. The value of h_0 is set as 0.001. The transmit power budget p_0 is set as 200 mW. The pathloss exponent α is set as 2.2. The noise figure at the server

²https://web.eece.maine.edu/~vweaver/group/green_machines.html

is 5 dBi, and the noise figure at the workers is 15 dBi. The system bandwidth is 200 KHz, and the power spectrum density is $10^{-17.4}$ mW/Hz.

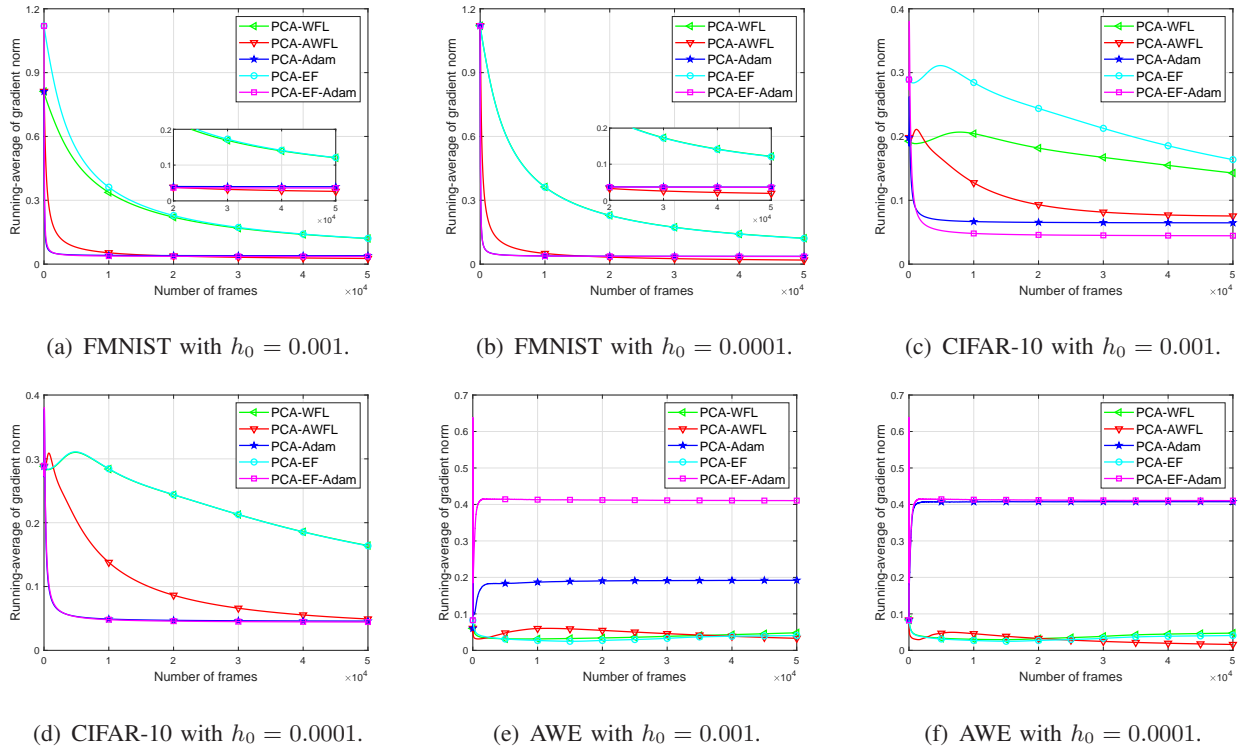


Fig. 3: The running-average of the gradient norm for the FMNIST, CIFAR-10 and AWE datasets.

Figure 3 shows the running-average of gradient norm after 5×10^4 frames for the PCA-WFL, PCA-AWFL, PCA-Adam, PCA-EF, and PCA-EF-Adam algorithms over FMNIST, CIFAR-10, and AWE datasets. Figs. 3(a), 3(c), and 3(e) show the convergence of running-average of gradient norm when the truncation threshold h_0 is 0.001. Figures 3(b), 3(d), and 3(f) show the convergence of running-average of gradient norm when the truncation threshold h_0 is 0.0001. We observe that the gradient norm of our proposed PCA-AWFL algorithm converges after around 20,000 frames for FMNIST, 30,000 frames for CIFAR-10, and 30,000 frames from AWE while the PCA-EF and PCA-WFL algorithms converge after 50,000 frames. This observation verifies our theoretical results that the PCA-AWFL algorithm converges faster than the PCA-WFL algorithm in Theorem 2. Besides, we also observe that the gradient norms of PCA-Adam and PCA-EF-Adam algorithms decrease faster for the FMNIST and CIFAR-10 than the PCA-AWFL algorithm as shown in Figs 3(a)–3(d). This is because that the Adam-type algorithm benefits from the adaptive gradients [50]. However, we observe that the gradient norms of PCA-Adam and PCA-EF-Adam algorithms converge to larger values than our proposed PCA-AWFL algorithm for the AWE dataset. This observation shows that myopic usage

of adaptive gradients can lead to a destructive effect on the convergence behaviour. We also illustrate the destructive effect in Figs. 4(e) and 4(f).

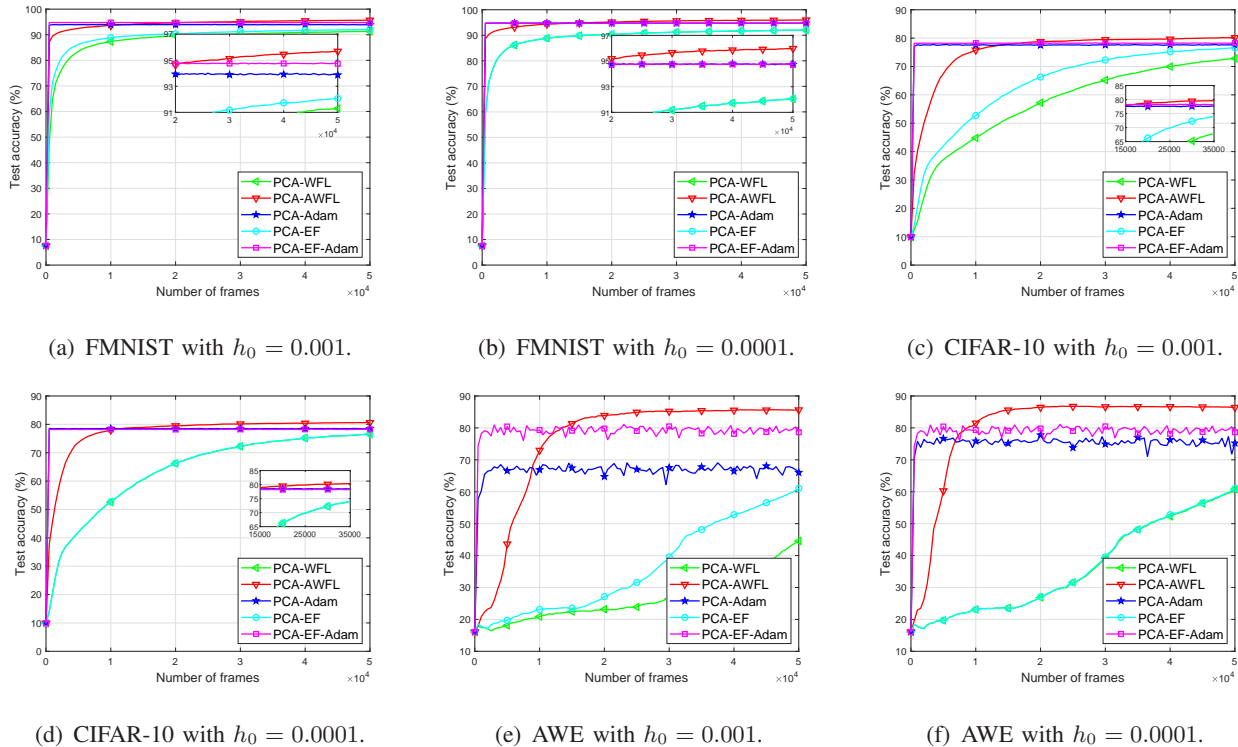


Fig. 4: The convergence behaviours of the testing accuracy for the FMNIST, CIFAR-10 and AWE datasets.

Figure 4 shows the convergence behaviours after 5×10^4 frames for the PCA-WFL, PCA-AWFL, PCA-Adam, PCA-EF, PCA-EF-Adam algorithms for FMNIST, CIFAR-10, and AWE datasets. From Fig. 4, we observe that the PCA-Adam and PCA-EF-Adam achieve the faster convergence rates and the lower testing accuracies than our proposed PCA-AWFL algorithm for the three datasets with $h_0 = 0.001$ and $h_0 = 0.0001$. Moreover, from Figs. 4(e) and 4(f), we observe that the several fluctuations in the testing accuracies of PCA-Adam and PCA-EF-Adam algorithms. This is due to the fact that the myopic usage of adaptive gradients induces Adam-type algorithms to stick to some local optimal models with the poorer quality compared with our proposed PCA-AWFL algorithm since the non-convex empirical risk has multiple local optimal models. When comparing Figs. 4(a), 4(c), and 4(e) with Figs. 4(b), 4(d), and 4(f), we observe that the required frames of our proposed PCA-AWFL algorithm decrease with the truncation threshold h_0 . This is due to the fact that a smaller value of h_0 grants the workers to upload more accurate global gradient estimators and thereby reduces the required frames for convergence. We also observe that the PCA-AWFL algorithm achieves the highest testing accuracy among the five algorithms. This is due to the fact that,

in each frame, the PCA-AWFL algorithm can use the historical aggregated gradients that contain more intelligence. By using more intelligence to adjust the searching direction of the model, the PCA-AWFL algorithm can achieve the best testing accuracy.

Figure 4 also shows that the gaps between our proposed PCA-AWFL algorithm and the benchmarks (i.e., PCA-EF and PCA-WFL algorithms) decrease as the number of frames becomes sufficiently large. Since the non-convex loss function has multiple local optimal models, we conclude that the model parameters of PCA-EF and PCA-WFL algorithms can converge to the neighbor of the local optimal models that have similar testing accuracy as the PCA-AWFL algorithm.

The convergence of gradient norms (in Fig. 3) and testing accuracies (in Fig. 4) jointly verify our envision: the testing accuracies of PCA-WFL and PCA-AWFL algorithms reach the peaks when the intelligence stops spreading.

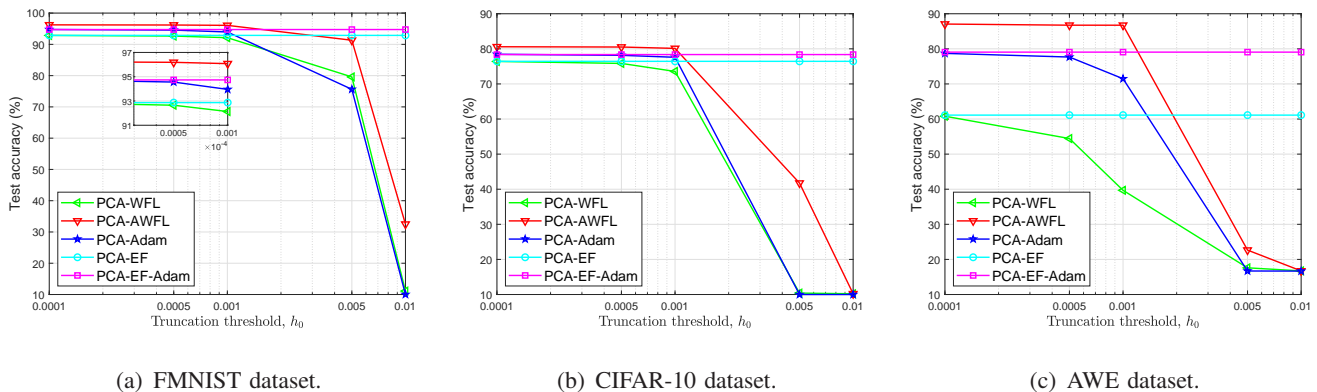


Fig. 5: Testing accuracy under different truncation thresholds for the FMNIST, CIFAR-10, and AWE datasets.

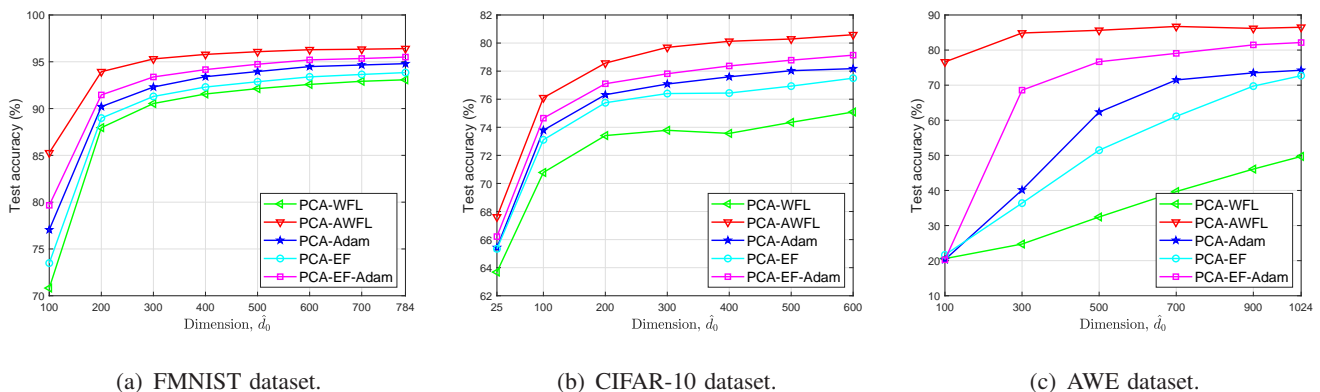


Fig. 6: Testing accuracy v.s. the dimension of data sample \hat{d}_0 for the FMNIST, CIFAR-10, and AWE datasets.

Figure 5 shows the impacts of truncation threshold h_0 on the testing accuracies for the PCA-WFL,

PCA-AWFL, PCA-Adam, PCA-EF, PCA-EF-Adam algorithms for FMNIST, CIFAR-10, and AWE datasets. We observe that our proposed PCA-AWFL algorithm achieves the highest testing accuracy under different truncation thresholds. Note that the PCA-EF and PCA-EF-Adam algorithms are insensitive to the truncation threshold since the local gradients are assumed to be uploaded over error-free channels. We observe that the accuracies of the PCA-WFL, PCA-AWFL, PCA-Adam algorithms monotonically decrease with the truncation threshold h_0 . This is due to the fact that a larger truncation threshold h_0 indicates a smaller chance of uploading local gradients such that a less accurate estimator of the global gradient is obtained at the server. A less accurate estimator of global gradient leads to a lower testing accuracy under the given number of frames.

Figure 6 shows the impacts of the one-shot distributed PCA on the testing accuracies of the PCA-WFL, PCA-AWFL, PCA-Adam, PCA-EF, PCA-EF-Adam algorithms for the FMNIST, CIFAR-10, and AWE datasets. Note that we select the reduced dimension \hat{d}_0 based on the numerical tests in Fig. 6. More specifically, we observe from Fig. 6(a) that reducing the sample dimension from 784 to 500 only sacrifices 0.34% testing accuracy for our proposed PCA-AWFL algorithm over the FMNIST dataset. The similar conclusions can be respectively obtained for the CIFAR-10 and AWE datasets from 6(b) and 6(c). Recalling Section II-A, we conclude that our proposed PCA-AWFL algorithm achieves a near optimal testing accuracy with communication expenditure reduced by $500/784 \approx 36.22\%$.

VI. CONCLUDING REMARKS

This work investigated the analog WFL system, where the workers have non-i.i.d. locations and upload local gradients to the server via orthogonal wireless channels. A one-shot distributed PCA had been used to reduce the dimension of local gradients, and the channel scheduling probability had been included in the truncated channel inversion to obtain an unbiased estimator of the aggregated gradient. Based on the one-shot PCA, truncated channel inversion and the Nesterov's momentum, the PCA-WFL and PCA-AWFL algorithms had been proposed. A finite-time analysis had been performed to quantify the convergence behaviours of the PCA-WFL and PCA-AWFL algorithms. Leveraging the intelligence networking, an intuition had been given to illustrate the existence of the speedup capability of Nesterov's momentum. Besides, the finite-time analysis had shown that the PCA-WFL and PCA-AWFL algorithms can achieve the parallel speedup with respect to the number of workers. Our proposed PCA-AWFL algorithm: 1) is more robust to the channel fadings and noise compared with the PCA-EF and PCA-WFL algorithms; 2) attains a higher testing accuracy compared with the state-of-the-art PCA-EF-Adam and PCA-Adam algorithms; 3) can be adapted to more practical datasets; 4) has a lower computational complexity per frame compared with the PCA-EF-Adam

and PCA-Adam algorithms. The only disadvantage of our proposed PCA-AWFL algorithm is the slower convergence behaviour compared with the PCA-Adam and PCA-EF-Adam algorithms over three datasets.

APPENDIX A

PROOF OF LEMMA 1

We first introduce two auxiliary inequalities before proceeding to prove the main results. The expectations of $c_{n,k} \mathbb{1}_{n,k} \odot y_{n,k}$ and $\|c_{n,k} \mathbb{1}_{n,k} \odot y_{n,k} - y_{n,k}\|^2$ are, respectively, derived as

$$\mathbb{E}[c_{n,k} \mathbb{1}_{n,k} \odot y_{n,k}] = c_{n,k} \mathbb{E}[\mathbb{1}_{n,k}] \odot y_{n,k} = y_{n,k} \quad (27)$$

and

$$\mathbb{E}[\|c_{n,k} \mathbb{1}_{n,k} \odot y_{n,k} - y_{n,k}\|^2] = (c_{n,k} - 1) \|y_{n,k}\|^2. \quad (28)$$

We also introduce a useful expectation $\mathbb{E}[\rho_{n,k}^{-2}]$ (See Appendix B for the detailed derivations) as

$$\mathbb{E}[\rho_{n,k}^{-2}] = p_0^{-1} \delta_{n,k}^\alpha \exp(-2\delta_{n,k}^\alpha h_0^2) E_1(\delta_{n,k}^\alpha h_0^2). \quad (29)$$

Recalling the condition $\frac{1}{N} \sum_{n=1}^N \|y_{n,k} - \nabla f(w_k)\|^2 \leq G$ and using the fact $\|x + y\|^2 \leq 2\|x\|^2 + 2\|y\|^2$, we have

$$\frac{1}{N} \sum_{n=1}^N \|y_{n,k}\|^2 \leq 2G + 2\|\nabla f(w_k)\|^2. \quad (30)$$

Based on (27) and the zero-mean channel noise, we obtain $\mathbb{E}[\frac{1}{N} \sum_{n=1}^N \hat{\nabla}_{n,k}] = \frac{1}{N} \sum_{n=1}^N y_{n,k}$.

We derive the upper bound of the expectation of $\|\frac{1}{N} \sum_{n=1}^N \mathbb{1}_{n,k} \odot y_{n,k}\|^2$ as

$$\mathbb{E}\left[\left\|\frac{1}{N} \sum_{n=1}^N c_{n,k} \mathbb{1}_{n,k} \odot y_{n,k}\right\|^2\right] \quad (31a)$$

$$= \mathbb{E}\left[\left\|\frac{1}{N} \sum_{n=1}^N (c_{n,k} \mathbb{1}_{n,k} \odot y_{n,k} - y_{n,k} + y_{n,k})\right\|^2\right] \quad (31b)$$

$$= \mathbb{E}\left[\left\|\frac{1}{N} \sum_{n=1}^N (c_{n,k} \mathbb{1}_{n,k} \odot y_{n,k} - y_{n,k})\right\|^2\right] + \|\nabla f(w_k)\|^2 \quad (31c)$$

$$= \frac{1}{N^2} \sum_{n=1}^N \mathbb{E}[\|c_{n,k} \mathbb{1}_{n,k} \odot y_{n,k} - y_{n,k}\|^2] + \|\nabla f(w_k)\|^2 \quad (31d)$$

$$= \frac{1}{N^2} \sum_{n=1}^N (c_{n,k} - 1) \|y_{n,k}\|^2 + \|\nabla f(w_k)\|^2 \quad (31e)$$

$$\leq \frac{c_1}{2N} + \frac{1}{2N^2} \sum_{n=1}^N \|y_{n,k}\|^2 + \|\nabla f(w_k)\|^2 \quad (31f)$$

where the equality (31c) is based on $\mathbb{E}[\|X\|^2] = \mathbb{E}[\|X - \mathbb{E}[X]\|^2] + \|\mathbb{E}[X]\|^2$ and $\nabla f(w_k) = \frac{1}{N} \sum_{n=1}^N y_{n,k}$; the equality (31d) follows from the fact that the vectors $c_{n,k} \mathbb{1}_{n,k} \odot y_{n,k} - y_{n,k}$ are independent for workers with $\mathbb{E}[c_{n,k} \mathbb{1}_{n,k} \odot y_{n,k} - y_{n,k}] = 0$; the equality (31e) is based on (28); and, the inequality (31f) follows from $\langle x, y \rangle \leq \frac{1}{2}\|x\|^2 + \frac{1}{2}\|y\|^2$ and the triangle inequality with $c_1 := \frac{1}{N} \sum_{n=1}^N (c_{n,k} - 1)$.

The derivation for the upper bound of accumulated noise is as follows. We take expectation over the squared norm of accumulated noise per frame k as

$$\mathbb{E}[\|z_k\|^2] = \frac{1}{N^2} \sum_{n=1}^N \mathbb{E} \left[\frac{\|y_{n,k}\|^2}{\rho_{n,k}^2} \|z_{n,k}\|^2 \right] \quad (32a)$$

$$\leq \frac{1}{N^2} \sum_{n=1}^N d_1 \sigma^2 \mathbb{E} \left[\frac{\|y_{n,k}\|^2}{\rho_{n,k}^2} \right] \quad (32b)$$

$$\leq \frac{1}{2N^2} \sum_{n=1}^N \|y_{n,k}\|^2 + \frac{c_2 d_1 \sigma^2}{2N p_0} \quad (32c)$$

where equality (32a) follows from the fact that the additive white Gaussian noise vectors $[z_{n,k}]_{n=1}^N$ are i.i.d. with mean zero and covariance $\sigma^2 I$; the inequality (32b) follows from the fact that channel noise is independent of channel fading and the location of workers with $\mathbb{E}[\|z_{n,k}\|^2] = d_1 \sigma^2$; the inequality (32c) is obtained by $\langle x, y \rangle \leq \frac{1}{2}\|x\|^2 + \frac{1}{2}\|y\|^2$ and the triangle inequality with $c_2 := \frac{1}{N p_0} \sum_{n=1}^N \delta_{n,k}^\alpha \exp(2\delta_{n,k}^\alpha h_0^2) E_1(\delta_{n,k}^\alpha h_0^2)$.

Note that the channel noise z_k is independent of the channel fading per frame k and the channel fading, we have

$$\mathbb{E} \left[\left\| \frac{1}{N} \sum_{n=1}^N \hat{v}_{n,k} \right\|^2 \right] \quad (33a)$$

$$\leq \mathbb{E} \left[\left\| \frac{1}{N} \sum_{n=1}^N c_{n,k} \mathbb{1}_{n,k} \odot y_{n,k} \right\|^2 \right] + \mathbb{E}[\|z_k\|^2] \quad (33b)$$

$$\leq \frac{1}{N^2} \sum_{n=1}^N \|y_{n,k}\|^2 + \frac{c_1}{2N} + \frac{c_2 d_1 \sigma^2}{2N} + \|\nabla f(w_k)\|^2 \quad (33c)$$

$$\leq 2\|\nabla f(w_k)\|^2 + \frac{c_1 + c_2 d_1 p_0^{-1} \sigma^2 + 4G}{2N} \quad (33d)$$

where the inequality (33c) the facts in (31f) and (32c); and (33d) follows from (30) with $N \geq 2$.

APPENDIX B

DERIVATION OF (29)

When the power of channel coefficient satisfies $|h_{n,k}[i]| \geq h_0$, the channel i is scheduled for worker n per frame k . Following the channel alignment policy in (4), we have

$$\frac{|\mathbb{1}_{n,k}[i]y_{n,k}[i]|^2}{|h_{n,k}[i]|^2\|y_{n,k}\|^2} = \begin{cases} \frac{|y_{n,k}[i]|^2}{|h_{n,k}[i]|^2\|y_{n,k}\|^2}, & |h_{n,k}[i]| \geq h_0 \\ 0, & |h_{n,k}[i]| < h_0. \end{cases} \quad (34)$$

Recalling the fact that each $h_{n,k}[i]$ follows i.i.d. circularly symmetric complex Gaussian distribution $\mathcal{CN}(0, \delta_{n,k}^{-\alpha})$. The power of each $|h_{n,k}[i]|^2$ is i.i.d. exponentially distributed with probability density function as $\delta_{n,k}^\alpha \exp(-\delta_{n,k}^\alpha x)$, $\forall n$.

Expanding the term $\|p_{n,k} \odot \frac{y_{n,k}}{\|y_{n,k}\|}\|^2$ and leveraging the power budget constraint (3), we obtain

$$\rho_{n,k}^{-2} = \frac{c_{n,k}^2}{p_0} \sum_{i=1}^{d_1} \frac{|\mathbb{1}_{n,k}[i]y_{n,k}[i]|^2}{|h_{n,k}[i]|^2\|y_{n,k}\|^2}. \quad (35)$$

Given the gradient $y_{n,k}$ and location $\delta_{n,k}$, we have

$$\mathbb{E}[\rho_{n,k}^{-2}] = \frac{c_{n,k}^2}{p_0} \mathbb{E} \left[\sum_{i=1}^d \frac{|\mathbb{1}_{n,k}[i]y_{n,k}[i]|^2}{|h_{n,k}[i]|^2\|y_{n,k}\|^2} \middle| y_{n,k}, \delta_{n,k} \right] \quad (36a)$$

$$= \frac{c_{n,k}^2}{p_0} \sum_{i=1}^{d_1} \frac{|y_{n,k}[i]|^2}{\|y_{n,k}\|^2} \int_{h_0^2}^{\infty} \frac{\delta_{n,k}^\alpha}{x \exp(\delta_{n,k}^\alpha x)} dx \quad (36b)$$

$$= \frac{c_{n,k}^2}{p_0} \sum_{i=1}^{d_1} \frac{|y_{n,k}[i]|^2}{\|y_{n,k}\|^2} \delta_{n,k}^\alpha E_1(\delta_{n,k}^\alpha h_0^2) \quad (36c)$$

$$= p_0^{-1} \delta_{n,k}^\alpha \exp(2\delta_{n,k}^\alpha h_0^2) E_1(\delta_{n,k}^\alpha h_0^2) \quad (36d)$$

where the inequality in (36b) follows from (34); the equality in (36c) follows from the definition of the exponential integral of $E_1(\cdot)$ in [51, pp. xxxv]; and, the equality in (36d) follows from the facts $\sum_{i=1}^{d_1} |y_{n,k}[i]|^2 / \|y_{n,k}\|^2 = 1$ and $c_{n,k} = \exp(\delta_{n,k}^\alpha h_0^2)$.

APPENDIX C

PROOF OF THEOREM 1

We start the proof by using the L -Lipschitz continuous condition as

$$f(w_{k+1}) - f(w_k) \leq \langle \nabla f(w_k), w_{k+1} - w_k \rangle + \frac{L}{2} \|w_{k+1} - w_k\|^2. \quad (37)$$

Based on the recursion (11), we have $\langle \nabla f(w_k), w_{k+1} - w_k \rangle = -\eta \langle \nabla f(w_k), \frac{1}{N} \sum_{n=1}^N \hat{\nabla}_{n,k} \rangle$. Taking expectation of $\langle \nabla f(w_k), \frac{1}{N} \sum_{n=1}^N \hat{\nabla}_{n,k} \rangle$ over the randomness of wireless channels and the locations of workers, we have

$$\mathbb{E}[\langle \nabla f(w_k), \frac{1}{N} \sum_{n=1}^N \hat{\nabla}_{n,k} \rangle] = \mathbb{E}[\|\nabla f(w_k)\|^2]. \quad (38a)$$

where the equality (38a) follows from the facts $\mathbb{E}[\mathbb{E}[X]] = \mathbb{E}[X]$ and Lemma 1.

Therefore, the expectation of the first term on the RHS of (37) is

$$\mathbb{E}[\langle \nabla f(w_k), w_{k+1} - w_k \rangle] = -\eta \mathbb{E}[\|\nabla f(w_k)\|^2]. \quad (39)$$

The expectation of the second term on the RHS of (37) is derived as

$$\mathbb{E}\left[\frac{L}{2} \|w_{k+1} - w_k\|^2\right] \quad (40a)$$

$$= \frac{\eta^2 L}{2} \mathbb{E}\left[\left\|\frac{1}{N} \sum_{n=1}^N \hat{\nabla}_{n,k}\right\|^2\right] \quad (40b)$$

$$\leq \eta^2 L \|\nabla f(w_k)\|^2 + \frac{c_1 + c_2 d_1 p_0^{-1} \sigma^2 + G}{4N} \eta^2 L \quad (40c)$$

where the equality (40c) follows from the recursion (11); and the inequality (40c) follows from Lemma 1.

Substituting (39) and (40c) into the expectation of (37), we obtain

$$\begin{aligned} & \mathbb{E}[f(w_{k+1}) - f(w_k)] \\ & \leq \eta(\eta L - 1) \mathbb{E}[\|\nabla f(w_k)\|^2] + \frac{c_1 + c_2 d_1 p_0^{-1} \sigma^2 + G}{4N} \eta^2 L. \end{aligned} \quad (41)$$

Dividing both sides of (41) by ηK and summing over $k = 0, \dots, K - 1$, we have

$$\begin{aligned} & \frac{1}{\eta K} \mathbb{E}[f(w_K) - f(w_0)] \\ & \leq \frac{\eta L - 1}{K} \sum_{k=0}^{K-1} \mathbb{E}[\|\nabla f(w_k)\|^2] + \frac{c_1 + c_2 d_1 p_0^{-1} \sigma^2 + G}{4N} \eta L. \end{aligned} \quad (42)$$

Setting $\eta \leq 3/4L$, we have $1 - \eta L \geq \frac{1}{4}$. Using the fact $f(x_K) \geq f^*$, we obtain

$$\begin{aligned} & \frac{1}{K} \sum_{k=0}^{K-1} \mathbb{E}[\|\nabla f(w_k)\|^2] \\ & \leq \frac{4}{\eta K} \mathbb{E}[f(w_0) - f^*] + \frac{c_1 + c_2 d_1 p_0^{-1} \sigma^2 + G}{N} \eta L. \end{aligned} \quad (43)$$

APPENDIX D

PROOF OF THEOREM 2

Before proceeding the proof, we set $x_0 = w_0$ and define an auxiliary sequence with $k \geq 1$ as

$$x_k = \frac{1}{1-\beta}w_k - \frac{\beta}{1-\beta}w_{k-1} + \frac{\eta\beta}{1-\beta} \frac{1}{N} \sum_{n=1}^N \hat{\nabla}_{n,k-1}. \quad (44)$$

Following several algebraic manipulations, we have

$$x_{k+1} - x_k = -\frac{\eta}{1-\beta} \frac{1}{N} \sum_{n=1}^N \hat{\nabla}_{n,k}, k \geq 0 \quad (45)$$

and

$$x_k - w_k = -\frac{\eta\beta^2}{1-\beta}u_k, k \geq 0. \quad (46)$$

Recalling (20) and summing $\|u_k\|^2$ over $k = 0, \dots, K-1$, we have

$$\sum_{k=0}^{K-1} \|u_k\|^2 = \sum_{k=1}^{K-1} \left\| \sum_{t=0}^{k-1} \beta^{k-1-t} \frac{1}{N} \sum_{n=1}^N \hat{\nabla}_{n,t} \right\|^2 \quad (47a)$$

$$= \sum_{k=1}^{K-1} s_k^2 \left\| \sum_{t=0}^{k-1} \frac{\beta^{k-1-t}}{s_k} \frac{1}{N} \sum_{n=1}^N \hat{\nabla}_{n,t} \right\|^2 \quad (47b)$$

$$\leq \sum_{k=1}^{K-1} \sum_{t=0}^{k-1} s_k \beta^{k-1-t} \left\| \frac{1}{N} \sum_{n=1}^N \hat{\nabla}_{n,t} \right\|^2 \quad (47c)$$

$$\leq \frac{1}{(1-\beta)^2} \sum_{t=0}^{K-1} \left\| \frac{1}{N} \sum_{n=1}^N \hat{\nabla}_{n,t} \right\|^2 \quad (47d)$$

where $s_k := \sum_{t=0}^{k-1} \beta^{k-1-t} = \frac{1-\beta^k}{1-\beta}$ in (47b); inequality (47c) follows from the convexity of ℓ_2 -norm; inequality (47d) follows from $\sum_{k=t+1}^{K-1} s_k \beta^{k-1-t} \leq \frac{1}{(1-\beta)^2}$.

Using the L -Lipschitz continuous property in Condition 2, we have

$$f(x_{k+1}) - f(x_k) \leq \langle \nabla f(x_k), x_{k+1} - x_k \rangle + \frac{L}{2} \|x_{k+1} - x_k\|^2. \quad (48)$$

Different from the proof in Theorem 1, we split the RHS of (48) into the sum of the following three terms

$$\langle \nabla f(x_k) - \nabla f(w_k), x_{k+1} - x_k \rangle \quad (49a)$$

$$\langle \nabla f(w_k), x_{k+1} - x_k \rangle \quad (49b)$$

$$\frac{L}{2} \|x_{k+1} - x_k\|^2. \quad (49c)$$

The expectation of (49a) is derived as

$$\mathbb{E}[\langle \nabla f(x_k) - \nabla f(w_k), x_{k+1} - x_k \rangle] \quad (50a)$$

$$= \frac{\eta}{1-\beta} \mathbb{E}[\langle \nabla f(w_k) - \nabla f(x_k), \frac{1}{N} \sum_{n=1}^N \hat{\nabla}_{n,k} \rangle] \quad (50b)$$

$$= \frac{\eta}{1-\beta} \mathbb{E}[\langle \nabla f(w_k) - \nabla f(x_k), \nabla f(w_k) \rangle] \quad (50c)$$

$$\leq \frac{\eta}{2(1-\beta)} \left[\frac{L^2}{a} \mathbb{E}[\|w_k - x_k\|^2] + a \mathbb{E}[\|\nabla f(w_k)\|^2] \right] \quad (50d)$$

$$= \frac{\eta}{2(1-\beta)} \left[\frac{\eta^2 L^2 \beta^4}{a(1-\beta)^2} \mathbb{E}[\|u_k\|^2] + a \mathbb{E}[\|\nabla f(w_k)\|^2] \right] \quad (50e)$$

where the equality (50b) follows from the recursion (45); the equality (50c) is based on the fact $\frac{1}{N} \sum_{n=1}^N \mathbb{E}[\hat{\nabla}_{n,k}] = c_1 \nabla f(w_k)$ and $\mathbb{E}[\mathbb{E}[X]] = \mathbb{E}[X]$; the inequality (50d) follows from the L -Lipschitz continuous gradient of loss function and the fact $\langle x, y \rangle \leq \frac{1}{2a} \|x\|^2 + \frac{a}{2} \|y\|^2$ with $a > 0$; and the equality (50e) is obtained via (46).

Following similar argument as (38) and recalling (45), the expectation of (49b) is derived as

$$\mathbb{E}[\langle \nabla f(w_k), x_{k+1} - x_k \rangle] = -\frac{\eta}{1-\beta} \mathbb{E}[\|\nabla f(w_k)\|^2]. \quad (51)$$

Substituting (45) into (49c), we obtain

$$\mathbb{E}\left[\frac{L}{2} \|x_{k+1} - x_k\|^2\right] = \frac{\eta^2 L}{2(1-\beta)^2} \mathbb{E}\left[\left\|\frac{1}{N} \sum_{n=1}^N \hat{\nabla}_{n,k}\right\|^2\right]. \quad (52)$$

Summing (50e), (51), and (52) and performing several algebraic manipulations, we obtain

$$\begin{aligned} & \mathbb{E}[f(x_{k+1}) - f(x_k)] \\ & \leq \frac{\eta}{1-\beta} \left[\frac{a}{2} - 1 \right] \mathbb{E}[\|\nabla f(w_k)\|^2] + \frac{\eta^3 L^2 \beta^4}{2a(1-\beta)^3} \mathbb{E}[\|u_k\|^2] + \frac{\eta^2 L}{2(1-\beta)^2} \mathbb{E}\left[\left\|\frac{1}{N} \sum_{n=1}^N \hat{\nabla}_{n,k}\right\|^2\right]. \end{aligned} \quad (53)$$

Summing (53) over $k = 0, \dots, K-1$ and recalling (20), we obtain

$$\begin{aligned} & \mathbb{E}[f(x_K) - f(x_0)] \\ & \leq \frac{\eta}{1-\beta} \left[\frac{a}{2} - 1 \right] \sum_{k=0}^{K-1} \mathbb{E}[\|\nabla f(w_k)\|^2] + \left[\frac{\eta^3 L^2 \beta^4}{2a(1-\beta)^3} + \frac{\eta^2 L}{2(1-\beta)^2} \right] \sum_{k=0}^{K-1} \mathbb{E}\left[\left\|\frac{1}{N} \sum_{n=1}^N \hat{\nabla}_{n,k}\right\|^2\right]. \end{aligned} \quad (54)$$

Setting $a = \frac{\eta L \beta^3}{(1-\beta)^2}$ and multiplying both sides of (54) by $\frac{1-\beta}{\eta}$, we obtain

$$\frac{1-\beta}{\eta} \mathbb{E}[f(x_K) - f(x_0)] \quad (55a)$$

$$\leq \left[\frac{\eta L \beta^3}{2(1-\beta)^2} - 1 \right] \sum_{k=0}^{K-1} \mathbb{E}[\|\nabla f(w_k)\|^2] + \frac{\eta L}{2(1-\beta)^2} \sum_{k=0}^{K-1} \mathbb{E}\left[\left\|\frac{1}{N} \sum_{n=1}^N \hat{\nabla}_{n,k}\right\|^2\right] \quad (55b)$$

$$\leq \left[\frac{\eta L (2 + \beta^3)}{2(1-\beta)^2} - 1 \right] \sum_{k=0}^{K-1} \mathbb{E}[\|\nabla f(w_k)\|^2] + \frac{c_1 + c_2 d_1 p_0^{-1} \sigma^2 + G}{4(1-\beta)^2 N} \eta L K \quad (55c)$$

where (55c) follows from Lemma 1.

Setting $\eta \leq \frac{3(1-\beta)^2}{2(2+\beta^3)L}$, we have $1 - \frac{\eta L(2+\beta^3)}{2(1-\beta)^2} \geq \frac{1}{4}$. Dividing both sides of (55c) by K and using $f(x_K) \geq f^*$, we obtain

$$\begin{aligned} & \frac{1}{K} \sum_{k=0}^{K-1} \mathbb{E}[\|\nabla f(w_k)\|^2] \\ & \leq \frac{4(1-\beta)}{\eta K} \mathbb{E}[f(x_0) - f^*] + \frac{c_1 + c_2 d_1 p_0^{-1} \sigma^2 + G}{(1-\beta)^2 N} \eta L. \end{aligned} \quad (56)$$

we complete the proof.

REFERENCES

- [1] F. R. Yu, "From information networking to intelligence networking: Motivations, scenarios, and challenges," *IEEE Network*, vol. 35, no. 6, pp. 209–216, Nov.-Dec. 2021.
- [2] X. Wang, Y. Han, V. C. M. Leung, D. Niyato, X. Yan, and X. Chen, "Convergence of edge computing and deep learning: A comprehensive survey," *IEEE Communications Surveys & Tutorials*, vol. 22, no. 2, pp. 869–904, Secondquarter 2020.
- [3] Y. Dong, J. Cheng, M. J. Hossain, and V. C. M. Leung, "Secure distributed on-device learning networks with Byzantine adversaries," *IEEE Network*, vol. 33, no. 6, pp. 180–187, Nov.-Dec. 2019.
- [4] T. Chen, G. B. Giannakis, T. Sun, and W. Yin, "LAG: Lazily aggregated gradient for communication-efficient distributed learning," in *Advances in Neural Information Processing Systems*, Montréal, CA, Dec. 2018, pp. 5050–5060.
- [5] J. Sun, T. Chen, G. B. Giannakis, Q. Yang, and Z. Yang, "Lazily aggregated quantized gradient innovation for communication-efficient federated learning," *IEEE Transactions on Pattern Analysis and Machine Intelligence*, vol. 44, no. 4, pp. 2031–2044, Apr. 2022.
- [6] Y. Dong, G. B. Giannakis, T. Chen, J. Cheng, M. J. Hossain, and V. C. M. Leung, "Communication-efficient robust federated learning over heterogeneous datasets," *arXiv:2006.09992*, June 2020.
- [7] H. Zhu and Q. Ling, "Bridging differential privacy and byzantine-robustness via model aggregation," *arXiv:2205.00107*, Apr. 2022.
- [8] X. Wang, R. Li, C. Wang, X. Li, T. Taleb, and V. C. M. Leung, "Attention-weighted federated deep reinforcement learning for device-to-device assisted heterogeneous collaborative edge caching," *IEEE Journal on Selected Areas in Communications*, vol. 39, no. 1, pp. 154–169, Jan. 2021.
- [9] X. Wang, C. Wang, X. Li, V. C. M. Leung, and T. Taleb, "Federated deep reinforcement learning for internet of things with decentralized cooperative edge caching," *IEEE Internet of Things Journal*, vol. 7, no. 10, pp. 9441–9455, Oct. 2020.
- [10] A. Zappone, M. Di Renzo, and M. Debbah, "Wireless networks design in the era of deep learning: Model-based, AI-based, or both?" *IEEE Transactions on Communications*, vol. 67, no. 10, pp. 7331–7376, Oct. 2019.
- [11] G. Zhu, D. Liu, Y. Du, C. You, J. Zhang, and K. Huang, "Toward an intelligent edge: Wireless communication meets machine learning," *IEEE Communications Magazine*, vol. 58, no. 1, pp. 19–25, Jan. 2020.
- [12] M. Salehi and E. Hossain, "Federated learning in unreliable and resource-constrained cellular wireless networks," *IEEE Transactions on Communications*, vol. 69, no. 8, pp. 5136–5151, Aug. 2021.
- [13] J. Xu and H. Wang, "Client selection and bandwidth allocation in wireless federated learning networks: A long-term perspective," *IEEE Transactions on Wireless Communications*, vol. 20, no. 2, pp. 1188–1200, Feb. 2021.
- [14] M. M. Amiri and D. Gündüz, "Machine learning at the wireless edge: Distributed stochastic gradient descent over-the-air," *IEEE Transactions on Signal Processing*, vol. 68, pp. 2155–2169, Mar. 2020.
- [15] Z. Zhang, G. Zhu, R. Wang, V. K. N. Lau, and K. Huang, "Turning channel noise into an accelerator for over-the-air principal component analysis," *IEEE Transactions on Wireless Communications*, vol. 21, no. 10, pp. 7926–7941, Oct. 2022.

- [16] M. Chen, Z. Yang, W. Saad, C. Yin, H. V. Poor, and S. Cui, "A joint learning and communications framework for federated learning over wireless networks," *IEEE Transactions on Wireless Communications*, vol. 20, no. 1, pp. 269–283, Jan. 2021.
- [17] W. Zhang, D. Yang, W. Wu, H. Peng, N. Zhang, H. Zhang, and X. Shen, "Optimizing federated learning in distributed industrial iot: A multi-agent approach," *IEEE Journal on Selected Areas in Communications*, vol. 39, no. 12, pp. 3688–3703, Dec. 2021.
- [18] J. He, S. Guo, M. Li, and Y. Zhu, "AceFL: Federated learning accelerating in 6G-enabled mobile edge computing networks," *IEEE Transactions on Network Science and Engineering*, to be published, July 2022.
- [19] J. Ren, G. Yu, and G. Ding, "Accelerating DNN training in wireless federated edge learning systems," *IEEE Journal on Selected Areas in Communications*, vol. 39, no. 1, pp. 219–232, Jan. 2021.
- [20] B. Xu, W. Xia, J. Zhang, T. Q. S. Quek, and H. Zhu, "Online client scheduling for fast federated learning," *IEEE Wireless Communications Letters*, vol. 10, no. 7, pp. 1434–1438, July 2021.
- [21] M. Zhang, G. Zhu, S. Wang, J. Jiang, Q. Liao, C. Zhong, and S. Cui, "Communication-efficient federated edge learning via optimal probabilistic device scheduling," *IEEE Transactions on Wireless Communications*, vol. 21, no. 10, pp. 8536–8551, Oct. 2022.
- [22] J. Liu, H. Xu, L. Wang, Y. Xu, C. Qian, J. Huang, and H. Huang, "Adaptive asynchronous federated learning in resource-constrained edge computing," *IEEE Transactions on Mobile Computing*, vol. 22, no. 2, pp. 674–690, Feb. 2023.
- [23] Z. Yang, M. Chen, W. Saad, C. S. Hong, and M. Shikh-Bahaei, "Energy efficient federated learning over wireless communication networks," *IEEE Transactions on Wireless Communications*, vol. 20, no. 3, pp. 1935–1949, Mar. 2021.
- [24] B. Yang, X. Cao, C. Huang, C. Yuen, M. Di Renzo, Y. L. Guan, D. Niyato, L. Qian, and M. Debbah, "Federated spectrum learning for reconfigurable intelligent surfaces-aided wireless edge networks," *IEEE Transactions on Wireless Communications*, vol. 21, no. 11, pp. 9610–9626, Nov. 2022.
- [25] X. Hou, J. Wang, C. Jiang, X. Zhang, Y. Ren, and M. Debbah, "UAV-enabled covert federated learning," *IEEE Transactions on Wireless Communications*, to be published, Feb. 2023.
- [26] Y. Du, S. Yang, and K. Huang, "High-dimensional stochastic gradient quantization for communication-efficient edge learning," *IEEE Transactions on Signal Processing*, vol. 68, pp. 2128–2142, Mar. 2020.
- [27] T. Sery, N. Shlezinger, K. Cohen, and Y. C. Eldar, "Over-the-air federated learning from heterogeneous data," *IEEE Transactions on Signal Processing*, vol. 69, pp. 3796–3811, June 2021.
- [28] D. Liu and O. Simeone, "Privacy for free: Wireless federated learning via uncoded transmission with adaptive power control," *IEEE Journal on Selected Areas in Communications*, vol. 39, no. 1, pp. 170–185, Jan. 2021.
- [29] G. Zhu, Y. Wang, and K. Huang, "Broadband analog aggregation for low-latency federated edge learning," *IEEE Transactions on Wireless Communications*, vol. 19, no. 1, pp. 491–506, Jan. 2020.
- [30] G. Zhu, Y. Du, D. Gündüz, and K. Huang, "One-bit over-the-air aggregation for communication-efficient federated edge learning: Design and convergence analysis," *IEEE Transactions on Wireless Communications*, vol. 20, no. 3, pp. 2120–2135, Mar. 2021.
- [31] M. M. Amiri and D. Gündüz, "Federated learning over wireless fading channels," *IEEE Transactions on Wireless Communications*, vol. 19, no. 5, pp. 3546–3557, May 2020.
- [32] R. Paul, Y. Friedman, and K. Cohen, "Accelerated gradient descent learning over multiple access fading channels," *IEEE Journal on Selected Areas in Communications*, vol. 40, no. 2, pp. 532–547, Feb. 2022.
- [33] T. Sery and K. Cohen, "On analog gradient descent learning over multiple access fading channels," *IEEE Transactions on Signal Processing*, vol. 68, pp. 2897–2911, Apr. 2020.
- [34] Y. Shao, D. Gündüz, and S. C. Liew, "Federated edge learning with misaligned over-the-air computation," *IEEE Transactions on Wireless Communications*, vol. 21, no. 6, pp. 3951–3964, June 2021.
- [35] D. Wen, G. Zhu, and K. Huang, "Reduced-dimension design of MIMO over-the-air computing for data aggregation in clustered IoT networks," *IEEE Transactions on Wireless Communications*, vol. 18, no. 11, pp. 5255–5268, Nov. 2019.

- [36] K. Yang, T. Jiang, Y. Shi, and Z. Ding, “Federated learning via over-the-air computation,” *IEEE Transactions on Wireless Communications*, vol. 19, no. 3, pp. 2022–2035, Mar. 2020.
- [37] A. Goldsmith, *Wireless Communications*. Cambridge University Press, 2005.
- [38] Y. Liang, M.-F. F. Balcan, V. Kanchanapally, and D. Woodruff, “Improved distributed principal component analysis,” in *Advances in Neural Information Processing Systems*, vol. 27, Montréal, CA, Dec. 2014.
- [39] H. Xiao, K. Rasul, and R. Vollgraf, “Fashion-MNIST: a novel image dataset for benchmarking machine learning algorithms,” *arXiv:1708.07747*, Aug. 2017.
- [40] A. Krizhevsky, “Learning multiple layers of features from tiny images,” Tech. Rep., 2009.
- [41] W. Zhang, D. Yang, Y. Xu, X. Huang, J. Zhang, and M. Gidlund, “Deephealth: A self-attention based method for instant intelligent predictive maintenance in industrial internet of things,” *IEEE Transactions on Industrial Informatics*, vol. 17, no. 8, pp. 5461–5473, Aug. 2021.
- [42] I. Jolliffe, *Principal component analysis*. Wiley Online Library, 2005.
- [43] D. Feldman, M. Schmidt, and C. Sohler, “Turning big data into tiny data: Constant-size coresets for k-means, PCA, and projective clustering,” *SIAM Journal on Computing*, vol. 49, no. 3, pp. 601–657, 2020.
- [44] R. Murray, B. Swenson, and S. Kar, “Revisiting normalized gradient descent: Fast evasion of saddle points,” *IEEE Transactions on Automatic Control*, vol. 64, no. 11, pp. 4818–4824, Nov. 2019.
- [45] Y. Nesterov, *Lectures on convex optimization (second edition)*. Springer, 2018, vol. 137.
- [46] F. Latorre, P. Rolland, and V. Cevher, “Lipschitz constant estimation of neural networks via sparse polynomial optimization,” in *International Conference on Learning Representations*, Virtual, Apr. 2020.
- [47] K. Yuan, B. Ying, and A. H. Sayed, “On the influence of momentum acceleration on online learning,” *Journal of Machine Learning Research*, vol. 17, no. 1, pp. 6602–6667, Oct. 2016.
- [48] A. Krizhevsky, I. Sutskever, and G. E. Hinton, “Imagenet classification with deep convolutional neural networks,” *Communications of the ACM*, vol. 60, no. 6, pp. 84–90, June 2017.
- [49] P. Molchanov, S. Tyree, T. Karras, T. Aila, and J. Kautz, “Pruning convolutional neural networks for resource efficient inference,” in *International Conference on Learning Representations*, Toulon, France, Apr. 2017.
- [50] X. Chen, S. Liu, R. Sun, and M. Hong, “On the convergence of a class of Adam-type algorithms for non-convex optimization,” in *International Conference on Learning Representations*, New Orleans, USA, May 2019.
- [51] A. Jeffrey and D. Zwillinger, *Table of Integrals, Series, and Products*. Academic Press, 2007.

Yanjie Dong (Member, IEEE) is with Shenzhen MSU-BIT university as an Associate Professor. Dr. Dong obtained his PhD and MASc degree from The University of British Columbia, Canada, in 2020 and 2016, respectively. His research interests focus on the protocol design of energy-efficient communications, machine learning based resource allocation algorithms, and quantum computing technologies. He regularly serves as a member of Technical Program Committee in flagship conferences in IEEE ComSoc.

Luya Wang received his Bachelor's degree from Shandong University of Science and Technology in 2020. He is pursuing a Master's degree in the School of Computer and Software at Shenzhen University, and is also a visiting student of Shenzhen MSU-BIT University, Shenzhen, China. His research interests focus on machine learning, federation learning, and wireless communications.

Yuanfang Chi (Student Member, IEEE) received the BSc. and MSc degrees from The University of British Columbia, Vancouver, BC, Canada, in 2012 and 2015, respectively, where she is currently pursuing the Ph.D. degree with the Department of Electrical and Computer Engineering. She is a visiting student of College of Computer Science and Software Engineering, Shenzhen University, Shenzhen, China. Her current research interests are distributed machine learning, knowledge graph, fault diagnosis, and Industrial Internet of Things.

Jia Wang (Member, IEEE) received her PhD degree in Electronic Engineering from City University of Hong Kong, Hong Kong SAR of China, in 2017. She is now an Assistant Professor with the College of Computer and Software Engineering, Shenzhen University. Her current research interests include lightweight security design for IoT and data security and privacy-preserving aspects of machine learning.

Haijun Zhang (Fellow, IEEE) is currently a Full Professor and Associate Dean in School of Computer and Communications Engineering at University of Science and Technology Beijing, China. He was a Postdoctoral Research Fellow in Department of Electrical and Computer Engineering, the University of British Columbia, Canada. He serves as an Editor of IEEE Transactions on Communications, and IEEE Transactions on Network Science and Engineering. He received the IEEE CSIM Technical Committee Best Journal Paper Award in 2018, IEEE ComSoc Young Author Best Paper Award in 2017, and IEEE ComSoc Asia-Pacific Best Young Researcher Award in 2019.

F. Richard Yu (Fellow, IEEE) received the PhD degree in electrical engineering from the University of British Columbia in 2003. His research interests include connected/autonomous vehicles, artificial intelligence, cybersecurity, and wireless systems. He has been named in the Clarivate Analytics list of "Highly Cited Researchers" since 2019, and received several Best Paper Awards from some first-tier conferences. He is an elected member of the Board of Governors of the IEEE VTS and Editor-in-Chief for IEEE VTS Mobile World newsletter. He is a Fellow of the IEEE, Canadian Academy of Engineering, Engineering Institute of Canada, and IET. He is a Distinguished Lecturer of IEEE in VTS and ComSoc.

Victor C. M. Leung (Life Fellow, IEEE) is a Distinguished Professor of Computer Science and Software Engineering at Shenzhen University, China. He is also an Emeritus Professor of Electrical and Computer Engineering and Director of the Laboratory for Wireless Networks and Mobile Systems at the University of British Columbia (UBC), Canada. His research is in the broad areas of wireless networks and mobile systems, and he has published widely in these areas. Dr. Leung is serving as a Senior Editor of the IEEE Transactions on Green Communications and Networking. He is also serving on the editorial boards of the IEEE Transactions on Cloud Computing, IEEE Transactions on Computational Social Systems, IEEE Access, IEEE Network, and several other journals. He received the 1977 APEBC Gold Medal, 1977-1981 NSERC Postgraduate Scholarships, IEEE Vancouver Section Centennial Award, 2011 UBC Killam Research Prize, 2017 Canadian Award for Telecommunications Research, 2018 IEEE TCGCC Distinguished Technical Achievement Recognition Award, and 2018 ACM MSWiM Reginald Fessenden Award. He co-authored papers that won the 2017 IEEE ComSoc Fred W. Ellersick Prize, 2017 IEEE Systems Journal Best Paper Award, 2018 IEEE CSIM Best Journal Paper Award, and 2019 IEEE TCGCC Best Journal Paper Award. He is a Life Fellow of IEEE, and a Fellow of the Royal Society of Canada (Academy of Science), Canadian Academy of Engineering, and Engineering Institute of Canada. He is named in the current Clarivate Analytics list of “Highly Cited Researchers”.

Xiping Hu (Member, IEEE) is currently a Distinguished Professor with Shenzhen MSU-BIT University, and is also with Beijing Institute of Technology, China. Dr. Hu received the Ph.D. degree from the University of British Columbia, Vancouver, BC, Canada. Dr. Hu is the co-founder and chief scientist of Erudite Education Group Limited, Hong Kong, a leading language learning mobile application company with over 100 million users, and listed as top 2 language education platform globally. His research interests include affective computing, mobile cyber-physical systems, crowdsensing, social networks, and cloud computing. He has published more than 150 papers in the prestigious conferences and journals, such as IJCAI, AAAI, ACM MobiCom, WWW, and IEEE TPAMI/TIP/TPDS/TMC/COMMAG.